Available online at www.sciencedirect.com
ScienceDirect
Trans. Nonferrous Met. Soc. China 23(2013) 3271−3279
Transactions of Nonferrous Metals Society of China
www.tnmsc.cn

Hot deformation behavior of Fe−29Ni−17Co alloy

Mohammad YAZDANI[1], Seyed Mehdi ABBASI[2], Ali Karimi TAHERI[1], Amir MOMENI[3]

1. Department of Materials Science and Technology, Sharif University of Technology, Tehran, Iran;
2. Metallic Materials Research Center (MMRC-MA), Tehran, Iran;
3. Department of Materials Science and Engineering, Hamedan University of Technology, Hamedan, Iran

Received 4 February 2013; accepted 3 June 2013

Abstract: Hot compression tests were carried out on a Fe−29Ni−17Co alloy in the temperature range of 900 °C to 1200 °C and at strain rates of 0.001−1 s^{-1}. Dynamic recrystallization was found responsible for flow softening during hot compression. The flow behavior was successfully analyzed by the hyperbolic sine equation and the corresponding material constants A, n and α were determined. The value of apparent activation energy was determined as 423 kJ/mol. The peak and steady state strains showed simple power-law dependence on the Zener−Hollomon parameter. The dynamic recrystallization kinetics was analyzed using Avrami equation and the corresponding exponent was determined to be about 2.7. This value, higher than 2 reported in the literatures, is associated with the mechanism of continuous dynamic recrystallization in the studied alloy. The flow curve up to the peak was modeled by the Cingara equation and the strain exponent, c, was determined about 0.85. The higher value of c compared with the value of 0.2 which has been reported for some stainless steels fortified the idea of extended dynamic recovery or continuous dynamic recrystallization in the studied alloy.

Key words: hot working; dynamic recrystallization; hot compression test; flow curve; modeling

1 Introduction

Fe−29Ni−17Co is a low expansion alloy which is widely used for glass-to-metal sealing purposes [1]. The thermal expansion coefficient of this alloy is comparable to that of glass and therefore the stress originated from differences in the expansion coefficients at the interface with a glass part is minimized.

LEE et al [2] reported that hot deformation regime could influence the alloy structure and its physical and/or mechanical characteristics. Theoretical explanations and experimental investigations have suggested that thermal expansion characteristics of Fe−29Ni−17Co may be affected by the microstructural conditions including residual strain as well as grain size [2]. It is known that the best combination of mechanical characteristics and thermal expansion is achieved when the microstructure is fine-grained.

It is generally accepted that a proper design of hot deformation and underlying restoration mechanisms can play an important role in modification of grain structure. Previous investigations on both ferrous (e.g. steels) and non-ferrous (e.g. Ti-alloys) alloys have proved that dynamic recrystallization (DRX) is the dominant restoration mechanism when low and medium stacking fault (SFE) materials are deformed at high temperatures [3−7]. The positive influence of DRX on flow softening and hot workability has been highlighted [8,9]. YAZDANI et al [10] conducted hot tensile tests on Fe−29Ni−17Co and found that good workability of the material at high temperatures is associated with DRX.

During hot working, DRX most frequently gives rise to grain refinement and therefore to the improvement of final mechanical properties. DING and GUO [11] showed that for DRX to start, the dislocation build-up should reach a critical value. KIM and YOO [12] and CHO and YOO [13] suggested that the critical dislocation density for the initiation of DRX is provided at a strain 0.6−0.8 times the peak strain of flow curve. After the peak, flow softening due to DRX finally attains a plateau associated with steady state deformation.

HUMPHREYS and HATHERLY [14] have stated that two processes are known responsible for the nucleation of DRX grains, strain induced grain boundary migration (SIBM) and subgrains growth. The mechanism

Corresponding author: Seyed Mehdi ABBASI; Fax: +98-21-22647033; E-mail: sma_abbasi@alborz.kntu.ac.ir
DOI: 10.1016/S1003-6326(13)62863-0

by which the DRX nucleus is formed depends on SFE. The progressive lattice rotation or extensive growth of subgrains towards the formation of liable DRX nuclei has been observed in high SFE materials such as ferrite, aluminum alloys and even some nickel alloys [15−17]. In low to medium SFE materials, the alternative process that termed as discontinuous DRX (DDRX) is initiated from the locally bulged or serrated boundaries of the pre-existing grains. At the early stages of DDRX, the new grains are preferentially formed at the grain boundaries and form a necklace structure that has been observed in hot deformation of ferrous and non-ferrous alloys [5,18]. Formation of new grains, irrespective of the underlying process leads to flow softening that is essential to hot working operation. When DRX grains totally consume the deformed structure, a dynamic balance between the work hardening and flow softening keeps the flow stress in a steady state condition. However, the mechanism of DRX determines the rate of softening and therefore plays an important role in proper design of an industrial process. The kinetics and the extent of DRX, therefore, depend strongly on the material characteristics and processing parameters. Although there is much information about DRX in different alloys, many issues have still remained unclear and the basic knowledge needs to be updated for every industrial alloy. The Fe−29Ni−17Co alloy has a very important role in different industries due to its unique physical characteristics. Although it has been proved that hot working has significant effects on the microstructure and thermal expansion of this alloy, its hot deformation behavior has been rarely documented. Thus, in current research hot compression tests have been conducted to address some unknown aspects of the hot deformation behavior of this alloy. The results of this investigation may facilitate the proper industrial design of hot working process.

2 Experimental

The material used in this investigation was a Fe−29Ni−17Co alloy having the chemical composition according to Table 1.

Table 1 Chemical composition of studied Fe−29Ni−17Co alloy

w(Ni)/%	*w*(Co)/%	*w*(Mn)/%	*w*(Si)/%
29.00	17.00	0.50	0.30
w(C)/%	*w*(S)/%	*w*(P)/%	*w*(Fe)/%
0.03	0.02	0.02	Bal.

The ingot of this alloy was sand cast and then refined by electro slag remelting (ESR) process. After homogenization heat treatment at 1100 °C for 3 h, the ingot was hot rolled 3 passes up to total reduction of 55%. The hot rolled strip with the final thickness of 24 mm was used to prepare hot compression samples. The starting microstructure of the hot rolled strip is shown in Fig. 1. Cylindrical compression specimens of 13.5 mm in height and 9 mm in diameter, were prepared according to the ASTM E209 standard with the axis along the rolling direction of the strip. Graphite powder was used to reduce friction between the specimen and anvil surfaces, and to minimize the sample barreling. An INSTRON 8502 testing machine equipped with a fully digital and computerized control furnace was employed to perform the hot compression tests at strain rates ranging from 0.001 s^{-1} to 1 s^{-1} at an interval of an order of magnitude and over temperature range of 900 °C to 1200 °C. For soaking, before testing specimens were held for 10 min at deformation temperature. After hot compression test, the specimens were cut along their longitudinal axes and prepared by the standard metallographic techniques for microstructural observations.

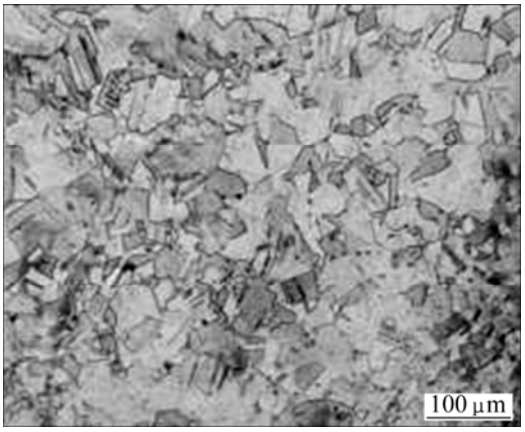

Fig. 1 Starting microstructure of studied Fe−29Ni−17Co alloy

3 Results and discussion

3.1 Flow curve analysis

Figure 2 exhibits typical flow curves plotted at different deformation regimes using the load—displacement results. It is obviously seen that the flow curves indicate the occurrence of DRX. The flow curve at 900 °C and 1 s^{-1} only comprises work hardening region and the peak point has shifted to higher strain. This behavior is typical at lower temperatures and higher strain rates where DRX is delayed due to low tendency for grain boundary migration. On the other hand, at high temperatures and low strain rates, the peak point is more discernible. Apart from the regime of 1100 °C and 0.001 s^{-1} which indicates a multi-peak flow curve, other flow curves are characterized by a single peak. The difference between multi-peak and single-peak behaviors is observed on the curves illustrated in Fig. 3. The 9th order polynomial used to regress the experimental data shows

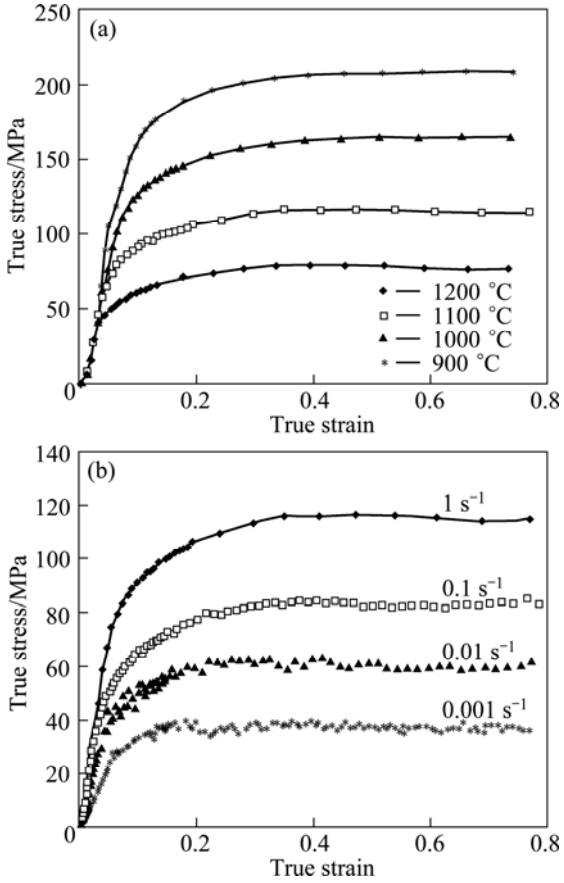

Fig. 2 True stress—strain curves at different deformation regimes: (a) Constant strain rate of 1 s^{-1}; (b) Constant temperature of 1100 °C

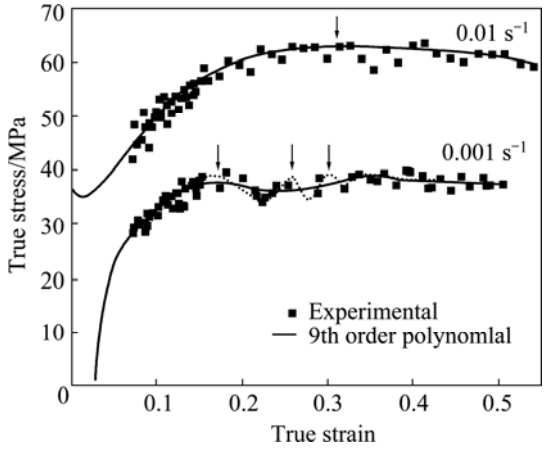

Fig. 3 Flow behavior at 1100 °C and strain rates of 0.001 s^{-1} and 0.01 s^{-1} indicating multi-peak and single-peak behaviors (The 9th order polynomial regression has been used to indicate the oscillation in the curves)

an oscillation at 0.001 s^{-1}, while at 0.01 s^{-1} a single distinct peak followed by steady state condition is observed. The positions of the peaks on the flow curve of 0.001 s^{-1} have been indicated by arrows. It is well known that multi-peak flow is often seen at high temperatures and low strain rates when a cycle of DRX is completed before the next one starts. On the contrary, single peak flow is seen when the successive cycles of DRX overlap. In a DRX flow curve, the peak and the onset of steady state condition are two important points that basically depend on the deformation variables. Theses characteristic points are usually determined by drawing the variation of work hardening rate ($d\sigma/d\varepsilon$) versus the flow stress or the applied strain as typically illustrated in Fig. 4. These points are the extremums of the flow curve and therefore corresponds to the points with zero work hardening rate. These laboratory results can be easily generalized to the industrial applications by developing simple equations that correlate the stress and strain of the peak and steady state condition to the deformation variables of strain rate and temperature. For industrial hot working processes, a workpiece is often subjected to strains high enough to reach the steady state. In addition, the steady state is a favorable region for shaping because of constant stress while the material is being deformed. Table 2 summarizes the characteristic strain and stress determined by the described method in Fig. 4 for different combinations of temperature and strain rate.

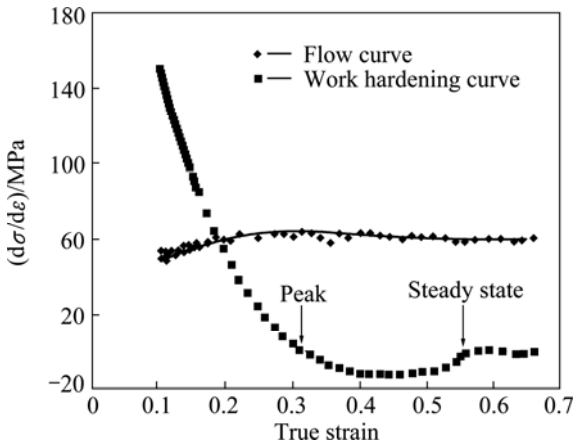

Fig. 4 Typical work hardening ($d\sigma/d\varepsilon$) curve superimposed on flow curve at 1100 °C and 0.01 s^{-1} to show position of peak point and onset of steady state condition at ($d\sigma/d\varepsilon$)=0

Table 2 Stress and strains of peak point and onset of steady state condition at different deformation regimes

Temperature/ °C	Strain rate/s^{-1}	Peak strain, ε_p	Peak stress, σ_p/MPa	Steady state strain, ε_p	Steady state stress, σ_p/MPa
900	0.001	0.46	98.2	0.7	97.2
1000	0.001	0.24	71.6	0.53	63
1100	0.01	0.31	62	0.57	58
1100	0.1	0.41	84	0.59	83
1200	0.1	0.27	57	0.5	53.1
1200	1	0.36	79.8	0.64	78

Figure 5 shows the variation of the steady state stress under different deformation conditions. The linear

curves in the logarithmic scale indicate that σ_s can be related to the strain rate by a power equation as follows [19]:

$$\sigma_s = K\dot{\varepsilon}^m \quad (1)$$

where m denotes the strain rate sensitivity of flow stress and K is a material constant. According to Eq. (1), the value of strain rate sensitivity (m) increases from 0.1 to 0.2 as temperature varies in the studied range. The observed increase in the value of m reflects better workability at higher temperatures.

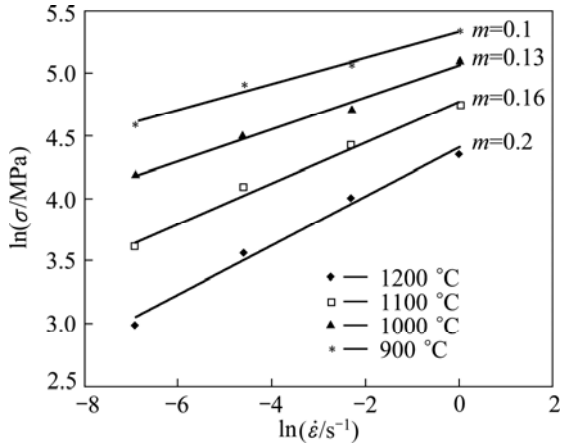

Fig. 5 Variation of steady state stress with strain rate to determine strain rate sensitivity

Many of previous researchers have used different constitutive equations to relate the flow stress to processing variables, i.e. temperature and strain rate. In this regard, FARNOUSH et al [20] and DUPREZ et al [21] have used the hyperbolic sine function originally proposed by GAROFALO [22]. It has been understood that except for very low or high stress levels, during hot deformation flow stress obeys the hyperbolic sine dependent on temperature and strain rate [23] as given by Eq. (2):

$$Z = \dot{\varepsilon}\exp(\frac{Q}{RT}) = A[\sinh(\alpha\sigma)]^n \quad (2)$$

where Z, Q and R denote the Zener−Hollomon parameter, the apparent activation energy of deformation and the gas constant, respectively; A, α and n are material constants which are determined from the empirical results by performing some algebraic operations on Eq. (2) as follows:

$$\ln\dot{\varepsilon} = (\ln A - \frac{Q}{RT}) + n\ln\sinh(\alpha\sigma) \quad (3)$$

Figure 6(a) indicates the variation of steady state stress with strain rate at different deformation temperatures. By linear regression, the average slop gives the value of n as 3.8. The value of α is also determined as 0.02 in a way that the curves become parallel. At a given strain rate, Eq. (3) can be written as Eq. (4):

$$\ln\sinh(\alpha\sigma_{ss}) = (\frac{\ln\dot{\varepsilon} - \ln A}{n}) + \frac{Q}{nRT} \quad (4)$$

The above equation is used to assess the empirical values of Q and A. Figure 6(b) shows the variations of flow stress with reciprocal temperature. According to Eq. (4), the average slop of linearly regressed data determines $Q/(nR)$. By this approach, Q is obtained as 423 kJ/mol, which is in agreement with the value reported by MOMENI et al [24] and FARNOUSH et al [20] for dynamic recrystallization of austenite in different stainless steel grades.

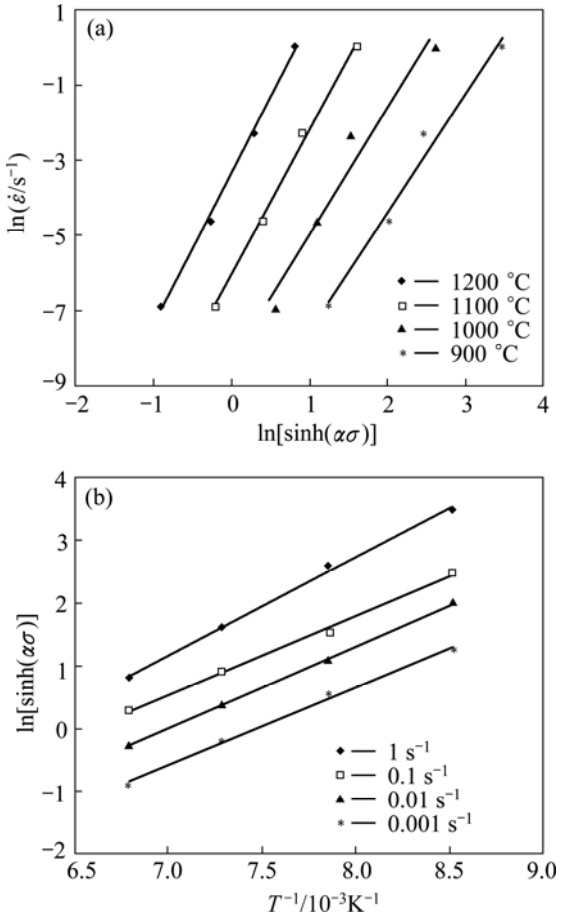

Fig. 6 Fitting of experimental data to hyperbolic sine function of n and α: (a) Q determination; (b) A determination

Figure 7 indicates the empirical data in the frame of the hyperbolic sine function. The linear regression of data with a good R-value shows the applicability of hyperbolic sine function to describe the flow behavior of the studied alloy. The experimental values obtained can be embraced as follows:

$$Z = \dot{\varepsilon}\exp(\frac{423000}{8.314T}) = 3.56\times10^{13}[\sinh(0.02\sigma)]^{3.8} \quad (5)$$

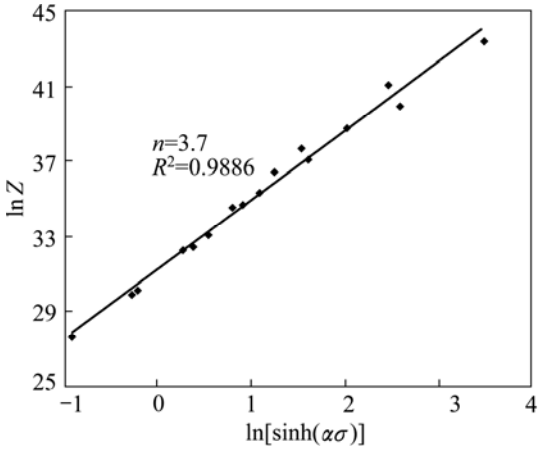

Fig. 7 Linear regression analysis of empirical data according to constitutive equation of hyperbolic sine function

Previous researches dealt with the characteristic strains of flow curve, peak and steady state strains and correlated them to the Zener−Hollomon parameter using simple power-law equations [8,25,26]. However, the exponents and constants are almost material-dependent and should be determined empirically. Figure 8 indicates the changes of strain and stress pertaining to the characteristic points (the peak and the onset of steady state condition) with Z parameter. The following equations best fit the empirical data:

$$\varepsilon_p = 0.0017Z^{0.16} \quad (6)$$

$$\varepsilon_s = 0.06Z^{0.07} \quad (7)$$

As clearly seen, the characteristic strains and stresses increase with Z, reflecting the fact that higher strain and stress are required for the initiation and completion of DRX at higher strain rates and lower temperatures. Moreover, it is worth noting that the peak and steady state stress are very closely related so that in the studied range of temperature and strain rate, the ratio of σ_p/σ_s is constantly 1.06. This, in turn, implies that the flow softening due to DRX is very small. The limited flow softening can be attributed to the higher extent of dynamic recovery (DRV). That is associated with the chemical composition of the studied alloy. It has been declared that Ni increases SFE in stainless steels and Ni−Co alloys while Co adversely decreases it [27]. As the austenite phase in this alloy is richer in Ni than Co, it is expected that SFE increases and the material becomes more prone to undergo DRV. Furthermore, the higher the SFE is, the easier the cross-slip and climb of dislocations known as the major micromechanisms of DRV are. Therefore, the extensive occurrence of DRV decreases the stored deformation energy that would be consumed by DRX and degrade its softening capacity.

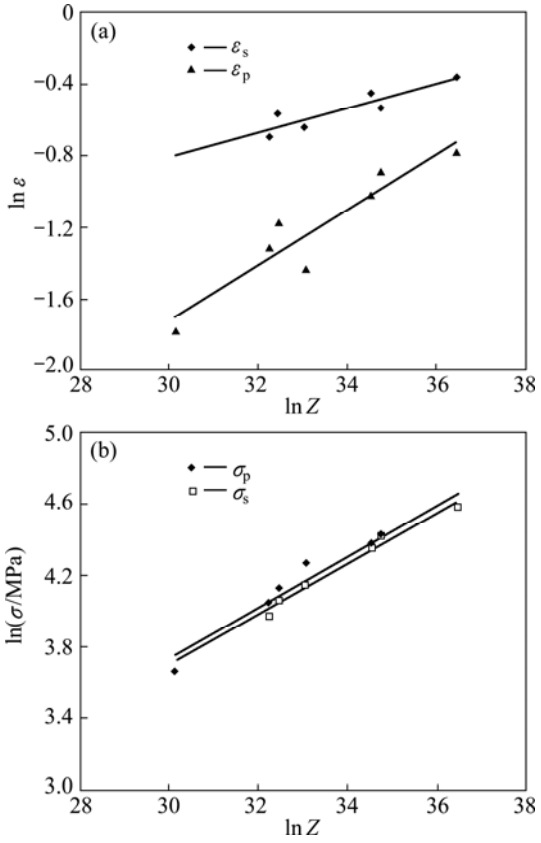

Fig. 8 Dependence of peak and steady state strain (a) and peak and steady state stress (b) to Z parameter in form of simple power relations

The above idea can be verified by the examination of the DRX kinetics. ROBERTS [28] proposed the kinetics of DRX using an Avrami-type equation as follows:

$$x_{DRX} = 1 - \exp[-\xi(\varepsilon - \varepsilon_c)^{\eta}] \quad (8)$$

where ε_c denotes the critical strain for the initiation of DRX and ξ and η are the material constants. In order to assess the average kinetics of DRX from the empirical data, a simplified equation can be used as follows [29]:

$$x_{DRX} = \frac{\sigma_p - \sigma}{\sigma_p - \sigma_s} = 1 - \exp[-k(\frac{\varepsilon - \varepsilon_p}{\dot{\varepsilon}})^n] \quad (9)$$

In Eq. (9), the peak of flow curve has been considered the starting point for the flow softening due to DRX. Therefore, the material constants k and n can be determined as the average slope and intercept in the plot of $\ln[1/(1-x)]$ vs $\ln[(\varepsilon-\varepsilon_p)/\dot{\varepsilon}]$ as shown in Fig. 9. From Fig. 9 the average value of n, known as Avrami's exponent, is obtained to be 2.7 which is higher than the value of 2 reported for DDRX in other steels [30]. It should be noted that the different values of n in the range of 1−4 are not uncommon dependent on the mechanism of nucleation, nucleation site and growth dimensionality. HUMPHREYS and HATHERLY [14] declared that when

n is in the range of 1−2, nucleation of new grains mostly occurs at grain boundaries at the early stages of DRX and further progress is controlled by the growth of recrystallized grains. This process is known as "site saturation" and leads to a necklace structure of new grains at the pre-existing grain boundaries. However, when n is in the range of 3−4, the nucleation of new grains is rather gradual during DRX [14]. This is the case when the gradual growth of subgrains during extended recovery links to continuous dynamic recrystallization (CDRX) in which coarse subgrains are introduced as the recrystallization nuclei. Referring to the value of n in the present research, it can be concluded that the dominant mechanism of DRX in the studied alloy is the extended recovery process and CDRX.

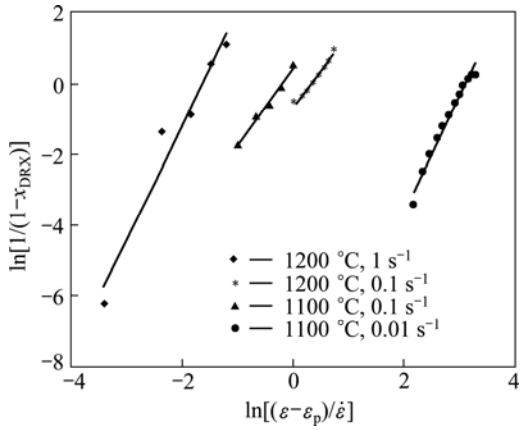

Fig. 9 Avrami plots showing variation of fractional softening due to DRX with strain

This mechanism of DRX in the studied alloy can be also verified by studying the flow behavior before the peak. In order to analyze the flow behavior of a material up to the peak point, the model proposed by CINGARA and McQUEEN can be used. CINGARA and McQUEEN [31] proposed the following exponential equation for the modeling of the flow curves of austenitic stainless steels up to the peak point:

$$\frac{\sigma}{\sigma_p}=[(\varepsilon/\varepsilon_p)\exp(1-\varepsilon/\varepsilon_p)]^c \quad (10)$$

where c is a material constant and is determined empirically. According to the linear regression of data in Fig. 10, c takes the average value of 0.85. Comparing with the value of 0.2 reported by CINGARA and McQUEEN [32] for most of stainless steels, a higher c value obtained here relies on the lower work hardening rate which may be imparted by a higher rate of DRV in the studied alloy. Figure 11 typically exhibits the prediction of work hardening region of the flow curve with two different c values. It manifests that the higher the c value, the greater the deformation resistance of the material. Furthermore, low deformation resistance at high temperatures signifies the contribution of DRV to the decrease of work hardening rate. Therefore, this analysis also corroborates the occurrence of CDRX in the studied alloy.

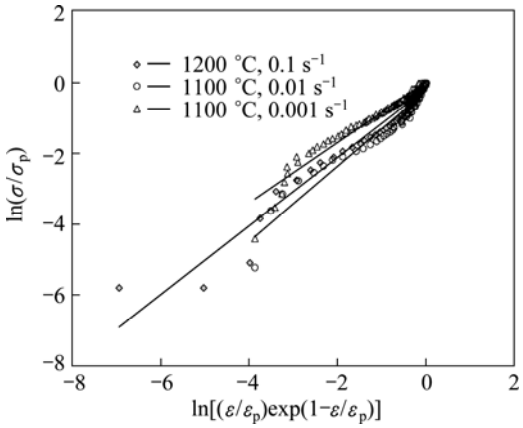

Fig. 10 Cingara plots to model variation of flow stress with strain in work hardening region

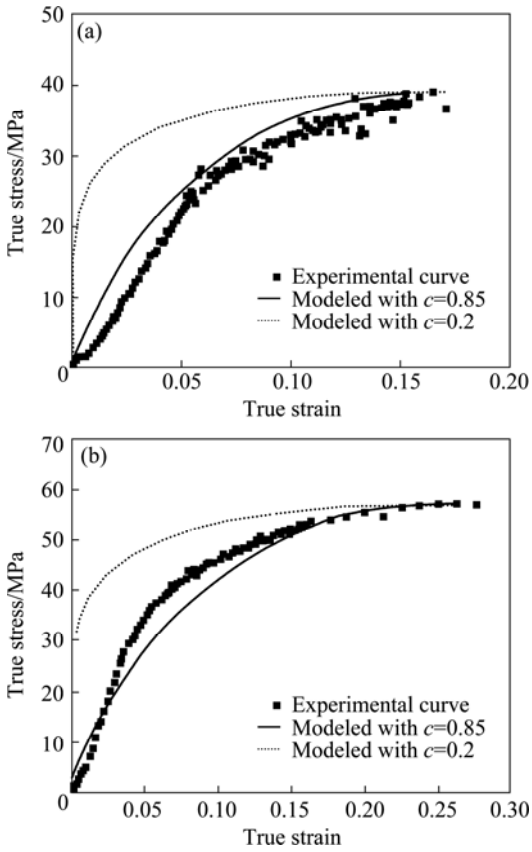

Fig. 11 Modeling flow curve at 1100 °C , 0.001 s^{-1} (a) and 1200 °C, 0.1 s^{-1} (b) by Cingara equation with two different c values of 0.2 proposed in literature [32] for stainless steels and 0.85 obtained for studied alloy

3.2 Microstructural characterization

Figure 12 demonstrates the microstructures obtained

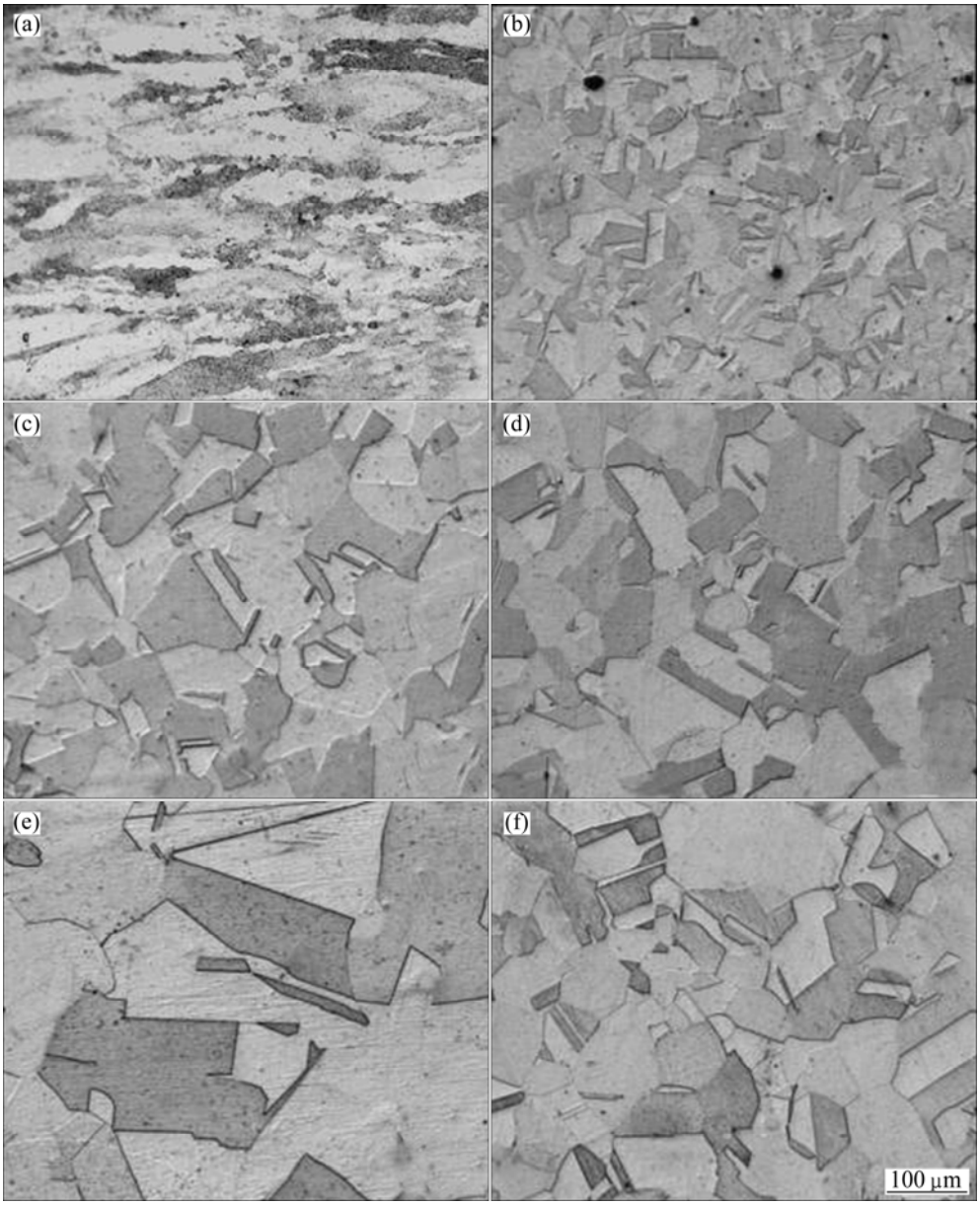

Fig. 12 Microstructures of samples hot deformed at 900 °C and 0.01 s^{-1} (a), 900 °C and 0.1 s^{-1} (b), 1100 °C and 0.01 s^{-1} (c), 1100 °C and 0.1 s^{-1} (d), 1200 °C and 0.01 s^{-1} (e), and 1200 °C and 0. 1 s^{-1} (f)

at different deformation regimes. The equiaxed small grains in most of micrographs are typical of DRX. As expected and is observed in Figs. 12(b) to (f), a finer grain structure is obtained as strain rate increases or temperature declines.

Figure 12(a) indicates that at 900 °C and strain rate of 0.01 s^{-1} the performed strain is not enough to cause a complete DRX. Using Eq. (6), the strains of the peak and the onset of steady state condition at 900 °C and 0.01 s^{-1} are calculated as 0.83 and 0.9, respectively. It is observed that, the total true strain of 0.7 performed in the compression tests is obviously between the critical strain for the initiation of DRX (ε_c=0.7ε_p) and the peak strain at 900 °C and 0.01 s^{-1}. The serrated boundaries in Fig. 12(a) near which new grains are discernible imply that DRX is at the early stages. The appearance of DRX grains near the preexisting grain boundaries and not necessarily on them can be regarded as another reason for the combination of the extended recovery and CDRX. It is well known that DDRX often leads to the formation of a necklace structure which is introduced as the occupation of grain boundaries by new grains at the early stages of recrystallization. Otherwise, when DRV occurs expeditiously, new grains are formed by the extended growth of subgrains through which the misorientation along the sub-boundaries gradually increases until transforming to high angle grain boundaries. In this case, it is suggested that the extended growth of subgrains

towards the formation of CDRX nuclei often occurs in certain positions of microstructure where there is a high orientation gradient [14]. Therefore, in the vicinity of prior grain boundaries where plastic deformation inhomogeneity is responsible for high orientation gradient, the nucleation of new grains is more expected, as shown in Fig. 12(a).

4 Conclusions

1) At temperatures higher than 900 °C, DRX is responsible for flow softening while at low temperatures, flow softening shifts to high strains.

2) The flow stress is successfully described by the hyperbolic sine constitutive equation and the material constants of A, n and α are determined as 3.56×10^{13}, 3.8 and 0.02, respectively.

3) The value of the apparent activation energy is determined as 423 kJ/mol.

4) The peak and steady state strains are related to the Zener−Hollomon parameter by simple power-law equations.

5) The kinetics of dynamic recrystallization complies with the Avrami equation. The Avrami power takes the value of 2.7. The difference between the obtained value and the value reported as 2 in the literatures can be attributed to the occurrence of continuous dynamic recrystallization in the studied alloy.

6) The work hardening stage of flow curve can be modeled by the Cingara equation and the value of c in the equation is determined approximately as 0.85. The high value of c comparing with 0.2 reported in the literature fortifies the occurrence of extended recovery or continuous dynamic recrystallization in the alloy.

Acknowledgements

The authors would like to thank the Research Board of Sharif University of Technology, Tehran, Iran for the provision of the research facilities used in this work.

References

[1] BRIAND D, WEBER P, de ROOIJ N F. Bonding properties of metals anodically bonded to glass [J]. Sensors and Actuators A, 2004, 114: 543−549.

[2] LEE K A, NAMKUNG J, KIM M C. Engineering plasticity and its applications from nanoscale to macroscale [C]// HUH H, PARK C G, LEE C S, KEUM Y T. Proceedings of the 9th AEPA 2008. Daejeon, Korea, 2008: 644−649.

[3] MOMENI A, ABBASI S M, SHOKUHFAR A. Hot compression behavior of as-cast precipitation-hardening stainless steel [J]. Can Metal Quart, 2007, 4: 189−193.

[4] MOMENI A, SHOKUHFAR A, ABBASI S M. Dynamic recrystallization of a Cr−Ni−Mo−Cu−Ti−V precipitation hardenable stainless steel [J]. J Mater Sci Technol, 2007, 23: 775−778.

[5] SHA W, MALINOV S. Modelling of microstructure, properties and applications [M]. Cambridge, UK: Woodhead Publishing, 2009.

[6] FURUHARA T, POORGANJI B, ABE H, MAKI T. Dynamic recovery and recrystallization in titanium alloys by hot deformation [J]. JOM, 2007, 59: 64−67.

[7] McQUEEN H J. Development of dynamic recrystallization theory [J]. Mater Sci Eng A, 2004, 387−389: 203−208.

[8] MOMENI A, DEHGHANI K, EBRAHIMI G R, KESHMIRI H. Modeling the flow curve characteristics of 410 martensitic stainless steel under hot working condition [J]. Metall Mater Trans A, 2010, 41: 2898−2904.

[9] DEHGHAN-MANSHADI A, BARNETT M R, HODGSON P D. Recrystallization in AISI 304 austenitic stainless steel during and after hot deformation [J]. Mater Sci Eng A, 2008, 485: 664−672.

[10] YAZDANI M, ABBASI S M, MOMENI A, KARIMI TAHERI A. Hot ductility of a Fe–Ni–Co alloy in cast and wrought conditions [J]. Mater Des, 2011, 32: 2956−2962.

[11] DING R, GUO Z X. Coupled quantitative simulation of microstructural evolution and plastic flow during dynamic recrystallization [J]. Acta Mater, 2001, 49: 3163−3175.

[12] KIM S I, YOO Y C. Dynamic recrystallization behavior of AISI 304 stainless steel [J]. Mater Sci Eng A, 2001, 311: 108−113.

[13] CHO S H, YOO Y C. Hot rolling simulations of austenitic stainless steel [J]. J Mater Sci, 2001, 36: 4267−4272.

[14] HUMPHREYS F J, HATHERLY M. Recrystallization and related annealing phenomena [M]. 2nd ed, Netherland: Pergamon, 2004.

[15] CIZEK, P WYNNE B P, RAINFORTH W M. EBSD investigation of the effect of strain path changes on the microstructure and texture of duplex stainless steel during hot deformation [J]. J Phys, 2006, 26: 331−334.

[16] YANG X, MIURA H, SAKAI T. Continuous dynamic recrystallization in a superplastic 7075 Aluminum alloy [J]. Mater Tans, 2002, 43: 2400−2407.

[17] EBRAHIMI G R, MOMENI A, ABBASI S M, MONAJATI H. Constitutive analysis and processing map for hot working of a Ni−Cu alloy [J]. Met Mater Int, 2013, 19: 11−19.

[18] EBRAHIMI G R, KESHMIRI H, MOMENI A, MAZINANI M. Dynamic recrystallization behavior of a superaustenitic stainless steel containing 16%Cr and 25%Ni [J]. Mater Sci Eng A, 2011, 528: 7488−7493.

[19] HOSFORD W F, CADDEL R M. Metal forming, mechanics and metallurgy [M]. New York: Cambridge University Press, 2007.

[20] FARNOUSH H, MOMENI A, DEHGHANI K, AGHAZADEH MOHANDESI J, KESHMIRI H. Hot deformation characteristics of 2205 duplex stainless steel based on the behavior of constituent phases [J]. Mater Des, 2010, 31: 220−226.

[21] DUPREZ L, DE COOMAN B C, AKDUT N. Flow stress and ductility of duplex stainless steel during high temperature torsion deformation [J]. Metall Mater Trans A, 2002, 33: 1931−1938.

[22] GAROFALO F. Fundamentals of creep and creep-rupture in metals [M]. New York: Macmillan Company, 1965.

[23] MOMENI A, DEHGHANI K. Microstructural evolution and flow analysis during hot working of a Fe−Ni−Cr superaustenitic stainless steel [J]. Metall Mater Tran, 2011, 42: 1925−1932.

[24] MOMENI A, ABBASI S M, SHOKUHFAR A. Hot compression behavior of as-cast precipitation-hardening stainless steel [J]. J Iron Steel Res Int, 2007, 14: 66−70.

[25] MOMENI A, ABBASI S M. Effect of hot working on flow behavior of Ti–6Al–4V alloy in single phase and two phase regions [J]. Mater Des, 2010, 31: 3599−3604.

[26] DEHGHAN-MANSHADI A, BARNETT M R, HODGSON P D. Hot deformation and recrystallization of austenitic stainless steel: Part I. Dynamic recrystallization [J]. Metall Mater Trans A, 2008, 39: 1359−1370.

[27] DAVIES J R, et al. ASM specialty handbook: Nickel, cobalt, and their alloys [M]. Materials Park, Ohio: ASM International, 2000, 159.
[28] ROBERTS W. Dynamic changes that occur during hot working and their significance regarding microstructural development and hot workability [C]//KRUSS G. Deformation Processing and Structure. ASM Materials Science Seminar. Metals Park, Ohio: American Society for Metals, 1982: 109−184.
[29] MOMENI A, DEHGHANI K, KESHMIRI H, EBRAHIMI G R. Hot deformation behavior and microstructural evolution of a superaustenitic stainless steel [J]. Mater Sci Eng A, 2010, 527: 1605−1611.
[30] DIETER G E, KUHN H A, SEMIATIN S L. Handbook of workability and process design [M]. Materials Park, Ohio: ASM International, 2003: 35.
[31] CINGARA A, McQUEEN H J. Calculating flow curves from high temperature constitutive data for 300 austenitic steels [J]. J Mater Process Technol, 1992, 36: 31−42.
[32] CINGARA A, McQUEEN H J. New method for determining sinh constitutive constants for high temperature deformation of 300 austenitic steels [J]. J Mater Process Technol, 1992, 36: 17−30.

Fe−29Ni−17Co 合金的热变形行为

Mohammad YAZDANI[1], Seyed Mehdi ABBASI[2], Ali Karimi TAHERI[1], Amir MOMENI[3]

1. Department of Materials Science and Technology, Sharif University of Technology, Tehran, Iran;
2. Metallic Materials Research Center (MMRC-MA), Tehran, Iran;
3. Department of Materials Science and Engineering, Hamedan University of Technology, Hamedan, Iran

摘　要：在实验温度为 900~1200 °C，应变率为 0.001~1 s^{-1} 的条件下，对 Fe−29Ni−17Co 合金进行热压缩试验。热压缩过程中的动态再结晶导致材料的流变软化。用双曲正弦方程分析材料的流变行为，并确定了相应的材料常数 A, n 和 α，其中得到的表观活化能为 423 kJ/mol。材料的应力峰值与稳态应力对 Zener−Hollomon 参数显示出简单的指数依赖关系。用 Avrami 方程分析了动态再结晶动力学，得到相应的指数为 2.7，高于文献报道的 2，这与连续动态再结晶机制有关。采用 Cingara 方程搭建峰值流变曲线，得到应变指数 c 约为 0.85，比有关报道的不锈钢的 c 值 0.2 高，这点更加强了关于进行 Fe−29Ni−17Co 合金动态回复或连续动态再结晶研究的想法。

关键词：热加工；动态再结晶；热压缩试验；流变曲线；建模

(Edited by Hua YANG)